ORIGINAL PAPER

In situ green synthesis of iron nanoparticles on PVA nanofiber and its application in adsorptive removal methylene blue

Mahdi Filsara[1] · Zahra-Beagom Mokhtari-Hosseini[1] · Masoumeh Mansoori-Rashvanloo[1]

Abstract

This study presents a novel approach for environmentally friendly paint removal, focusing on the efficient removal of methylene blue from aqueous environments using iron nanoparticles embedded in polyvinyl alcohol nanofibers. Iron nanoparticles were synthesized via a green method employing green tea extract under optimized conditions and characterized by FESEM, DLS, TGA, DTG, EDS, FTIR, and XRD. The average size of synthesized iron nanoparticles was 22 nm. Two fabrication techniques were employed to embed the nanoparticles into polyvinyl alcohol nanofibers: electrospinning of a solution containing iron nanoparticles, and in situ synthesis of nanoparticles on the PVA nanofibers. Comparative analyses revealed superior methylene blue adsorption rates when nanoparticles were synthesized in situ on the nanofibers. Characterization techniques, including FESEM, XRD, and FTIR, confirmed the successful formation of nanoparticles on the nanofibers. Response surface method using central composite design (CCD) was performed to find the optimal removal conditions. Optimal removal (85%) occurred under adsorption conditions of pH 8.6, an initial methylene blue concentration of 30 mg/L, a nanofiber dose of 1.6 g/L, and a contact time of 100 min. Kinetic studies demonstrated a pseudo-second-order adsorption model, while Langmuir isotherm analysis indicated a maximum adsorption capacity of 24.509 mg/g. Thermodynamic analysis suggested the spontaneous and exothermic nature of the adsorption process. This composite membrane is an efficient and economical method for removal dye from wastewaters.

Keywords Green synthesis · Adsorption · Nanofibers · Polyvinyl alcohol (PVA) · Methylene blue

✉ Zahra-Beagom Mokhtari-Hosseini
z.mokhtari@hsu.ac.ir

1 Department of Chemical Engineering, Faculty of Petroleum and Petrochemical Engineering, Hakim Sabzevari University, Sabzevar, Iran

🖄 Springer

Introduction

Water is an indispensable resource for all living organisms, and its contamination by pollutants poses significant environmental and public health challenges. Among these pollutants, synthetic dyes are of particular concern due to their toxicity, persistence, and ubiquity in industrial effluents. These dyes are extensively utilized in various industries, including textiles, leather, paper, and food processing. Their complex aromatic structures are designed to resist degradation under environmental conditions such as light, temperature, and microbial activity, leading to their persistence in aquatic environments. The discharge of dye-laden wastewater into water bodies not only diminishes the aesthetic quality of these water sources but also poses severe health risks to aquatic life and human populations [1].

Methylene blue (MB) is one of the most commonly used synthetic dyes, particularly in the textile industry, where it is employed for dyeing materials such as cotton, wool, and silk. The widespread use of MB has resulted in its frequent detection in industrial effluents, raising significant environmental and health concerns. As a cationic dye that is highly soluble in water, MB can have toxic effects on aquatic organisms and presents potential health risks to humans through exposure to contaminated water. High concentrations of MB can lead to health issues like eye irritation, respiratory problems, vomiting, severe jaundice, shock, dizziness, necrosis, methemoglobinemia, and sweating [2–6]. Furthermore, the resistance of MB to conventional water treatment processes exacerbates its environmental impact, as it can persist in aquatic ecosystems, leading to long-term contamination. This persistence underscores the urgent need for the development and implementation of more effective and biocompatible methods for the removal of MB and similar pollutants from water sources. Addressing this issue is critical for safeguarding public health and maintaining the integrity of aquatic ecosystems.

Various methods are employed to remove dyes from aqueous solutions, including chemical, physical, biological, and combined techniques. Recently, the use of nanoparticles in eliminating water pollutants has gained prominence. Nonetheless, employing these nanoparticles without a recycling strategy can result in secondary pollution in groundwater posttreatment. Iron nanoparticles (INPs) are popularly used for their high adsorption capacity, particularly for dyes. However, the synthesis of INPs using toxic reducing agents like sodium borohydride poses significant environmental risks [7].

The green synthesis of nanoparticles offers an eco-friendly, cost-effective, and recyclable alternative, gaining importance in contemporary times. This method utilizes aqueous extracts from various plants as reducers and stabilizers in nanoparticle synthesis [8, 9]. Green tea stands out for synthesizing INPs among different plants due to its easy availability and high regenerative properties. Furthermore, using polymer nanofibers as iron nanoparticle carriers can mitigate secondary pollution following treatment [10–12]. Nanofibers, in particular, have garnered significant interest for their unique properties compared to traditional fibrous structures [13].

Polymer electrospinning is an economical and practical technique for producing nanofibers, which are characterized by their high specific surface area, high

porosity, stability in liquid phases, and excellent support for immobilizing iron nanoparticles [14, 15]. The expansive specific area of these nanofibers enables the iron nanoparticles to offer more reaction sites, thereby enhancing the reduction of pollutants and contributing to a more dispersed and smaller nanoparticle size. Additionally, the high porosity of the nanofibers facilitates effective contact between the iron nanoparticles and raw water, ensuring a relatively stable water flow [16].

PVA, a biocompatible synthetic polymer, is extensively utilized in biomedical sciences and engineering. However, its water solubility is a notable limitation. Consequently, cross-linking becomes indispensable in applications involving direct contact with water or aqueous mixtures to maintain stability and effectiveness [17, 18].

Polyvinyl alcohol (PVA) and its composites with other polymers have been widely recommended as effective carriers for nanoparticles in various studies. For example, Bayat et al. developed a chitosan/PVA nanocomposite embedded with polyaniline/silica hybrid nanostructures for the adsorption of organic dyes [19]. Similarly, Osei et al. utilized green-synthesized silver nanoparticles supported on natural rubber latex/PVA nanofibers for the efficient sorption of mercury. These studies highlight the versatility and efficacy of PVA-based materials in environmental remediation applications [20].

Extensive research has been conducted on the synthesis of nanoparticles on various nanofibers; however, there has been no investigation into the in situ synthesis of iron nanoparticles on polyvinyl alcohol (PVA) nanofibers using a green synthesis approach. Given the affordability and biocompatibility of PVA, coupled with the environmental advantages of green synthesis and the high adsorption capacity of iron nanoparticles, this study focuses on the development of this novel surface adsorbent. The research aims to evaluate its effectiveness in the adsorption of methylene blue, leveraging the synergistic properties of PVA nanofibers and iron nanoparticles.

Materials and methods

Material

Dry green tea was purchased from the herbal store, washed, and then dried. Ferrous sulfate heptahydrate ($FeSO_4.7H_2O$), polyvinyl alcohol (MW = 72,000), glutaraldehyde (25% wt), hydrochloric acid, and sodium hydroxide were purchased from Merck Chemicals Co., Ltd. Methylene blue (MB) was supplied by CARLO ERBA Reagents Co., Ltd. Double-distilled water was used in all step. All the reagents were used without further purification.

Leaf extract preparation and synthesis of INPs

Green tea leaves are ground into a powder using a household mill and then sifted through a specific mesh sieve. Five grams of these powdered tea leaves are mixed with 100 mL of double-distilled water in a 250-mL Erlenmeyer flask. This mixture

is then heated for 60 min on a hotplate stirrer at a temperature of 80 °C and a stirring speed of 300 rpm. After cooling, the extracts are filtered through filter paper to remove tea sludge. The filtrate is subsequently centrifuged at 10,000 rpm for 10 min to eliminate fine leaf particles. The resulting clear supernatant is stored in the refrigerator for future experiments. The pH of these extracts is adjusted using hydrochloric acid and sodium hydroxide (0.1M), following the design of the experiment data.

For the synthesis of iron nanoparticles, the prepared tea leaf extracts are added to 5 mL of a 0.1M $FeSO_4.7H_2O$ solution in predetermined volume ratios. This mixture is immediately placed in an incubator shaker set at a speed of 200 rpm. Upon mixing, the formation of zero-valent iron nanoparticles is indicated by the appearance of a black-colored precipitate [6, 18]. The reaction product is then centrifuged, and the resulting black precipitate is washed twice with double-distilled water and once with ethanol. This washing process aims to remove any unreacted plant chemicals and solutes. Finally, the precipitate is suspended in ethanol and left at room temperature for 15 h to dry the nanoparticles.

Fabrication of the PVA/INPs nanofiber

PVA/INPs nanofibers were fabricated by two methods. The production methods are shown in Fig. 1.

Method 1: In method 1, the specified amount of INPs was added to double-distilled water and stirred until it reached a homogenous consistency. Subsequently, PVA pellets were introduced and stirred at 80 °C for 4 h to ensure complete dissolution of the polymer. The nanofibers were produced via electrospinning after cooling to room temperature and removing air bubbles through an ultrasonic bath. This process involved a flow rate of 0.8 mL/h, a 9–15 kV voltage range, and a 12 cm distance between the needle and collector. The resultant PVA/INPs nanofibers were then
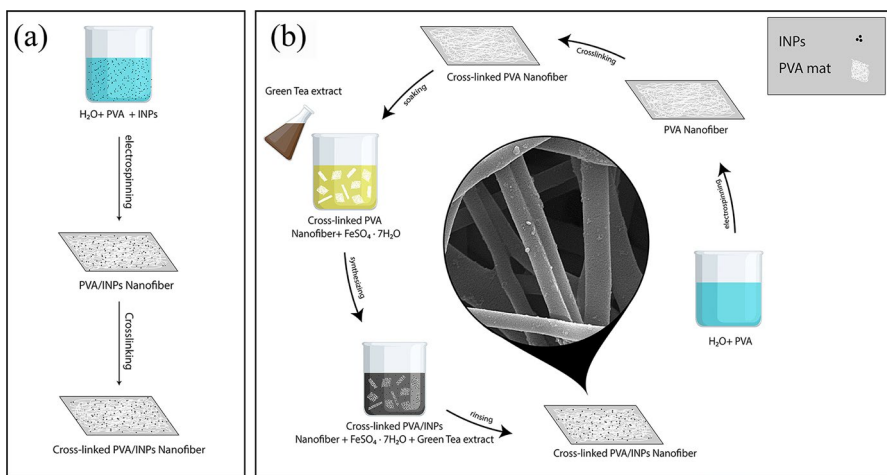

Fig. 1 PVA/INPs nanofiber fabrication methods: **a** method 1; and **b** method 2

dried at room temperature. Table 1 details the composition of the various nanofibers produced.

The nanofibers were treated with 25% glutaraldehyde and 37% HCL for cross-linking. Initially, a 10:1 mixture of glutaraldehyde and HCL was placed in a Petri dish inside a desiccator. The nanofibers were then positioned in the desiccator above the Petri dish, exposing them to glutaraldehyde vapor for reaction. This setup was placed in an oven, with the temperature first set to 80 °C for one hour, followed by 50 °C for seven hours [21, 22]. After the heat treatment, the cross-linked nanofibers were immersed in water twice, each for a duration of 10 min, and subsequently dried at room temperature.

Method 2: A 10% w/w PVA solution was prepared, electrospun, and cross-linked using method 1. Subsequently, the resultant cross-linked nanofibers were immersed in a 0.1 M $FeSO_4.7H_2O$ solution for an hour. After this incubation period, tea extract, produced under optimal conditions, was introduced into the solution containing the nanofibers, forming nanoparticles. The PVA/INPs nanofibers were then thoroughly washed—twice with double-distilled water and once with ethanol—to eliminate any excess materials. Finally, these were air-dried at room temperature.

Adsorption study

All experiments were conducted using a batch adsorption process to assess the efficacy of PVA/INPs nanofibers in removing methylene blue (MB). A specific quantity of PVA/INPs nanofibers was introduced into a predetermined concentration of MB solution. This process was carried out for a set duration at room temperature, with constant stirring at 150 rpm. Prior to adding the nanofibers, the pH of the MB solution was adjusted using 0.1 M HCl and NaOH to achieve the desired level. Upon completion of the contact time, the nanofibers were separated from the solution. The concentration of methylene blue in the residual solution was then determined using a UV–visible spectrophotometer at a wavelength of 668 nm. The percentage of dye removal, equilibrium adsorption capacity, and the adsorptive efficiency of the nanofibers were quantified using specific formulas.

$$Removal\,percentage\,(\%) = \frac{(c_0 - c_t)}{c_0} * 100 \tag{1}$$

$$q_e\left(mg.g^{-1}\right) = (c_0 - c_e)\frac{v}{w} \tag{2}$$

Composition	5%INPs	4%INPs	3%INPs
INPs (g)	0.370	0.296	0.223
PVA (g)	7.380	7.385	7.390
Water (g)	92.250	92.319	92.387

Table 1 The required amount of INPs to prepare PVA/INPs solutions

$$q_t\left(mg.g^{-1}\right) = (c_0 - c_t)\frac{v}{w} \tag{3}$$

where q_e is the adsorption capacity at equilibrium, q_t is the adsorption capacity at time t, C_t is the dye concentration at time t (mg/L), C_e is the equilibrium dye concentration in the solution, C_0 is the initial dye concentration (mg/L), W is the weight of the PVA/INPs nanofiber used (g), and V is the volume of dye solution used (L) [23, 24].

Process optimization

A design of experiments approach was employed to optimize the synthesis of INPs using green tea extract and the removal of methylene blue (MB) from aqueous solutions using PVA/INPs nanofibers. Specifically, the central composite design (CCD) within the response surface method was utilized for this purpose. Four variables were identified for optimization in each process. The levels for these variables were chosen based on insights gathered from preliminary experiments and findings reported in the literature [25–28]. A series of experiments were delineated using the Design Expert 13.0 software. The specific variables studied and their respective levels are detailed in Table 2. The analysis of the results was also performed using Design Expert 13.0 software.

Characterizations

The structural and morphological characteristics of nanoparticles and nanofibers were extensively analyzed using various techniques. Fourier transform infrared spectroscopy (FTIR) and X-ray diffraction (XRD) provided molecular and crystalline structure insights. The surface morphology was examined using a field-emission scanning electron microscope (FSEM), while the elemental composition was determined through energy-dispersive X-ray spectroscopy (EDS). Additionally, the

Table 2 The studied variables and their levels to optimizing the amount of INPs synthesis and removal percentage of MB

Variables	Low (−1)	Medium (0)	High (1+)
INPs synthesis			
pH	5	7	9
Temperature (°C)	40	45	50
Volume ratio of extract to salt	2	3	4
Time (min)	40	65	90
Removal of MB			
pH	5	7	9
Time (min)	50	90	130
Initial concentration (mg/L)	20	30	40
Dosage nanofiber (g/L)	0.6	1.1	1.6

size distribution of the nanoparticles was assessed using dynamic light scattering (DLS), and their thermal stability was evaluated through thermal gravimetric analysis (TGA). To measure the concentration of methylene blue (MB) in solutions, a UV–visible spectrophotometer was employed.

Results and discussion

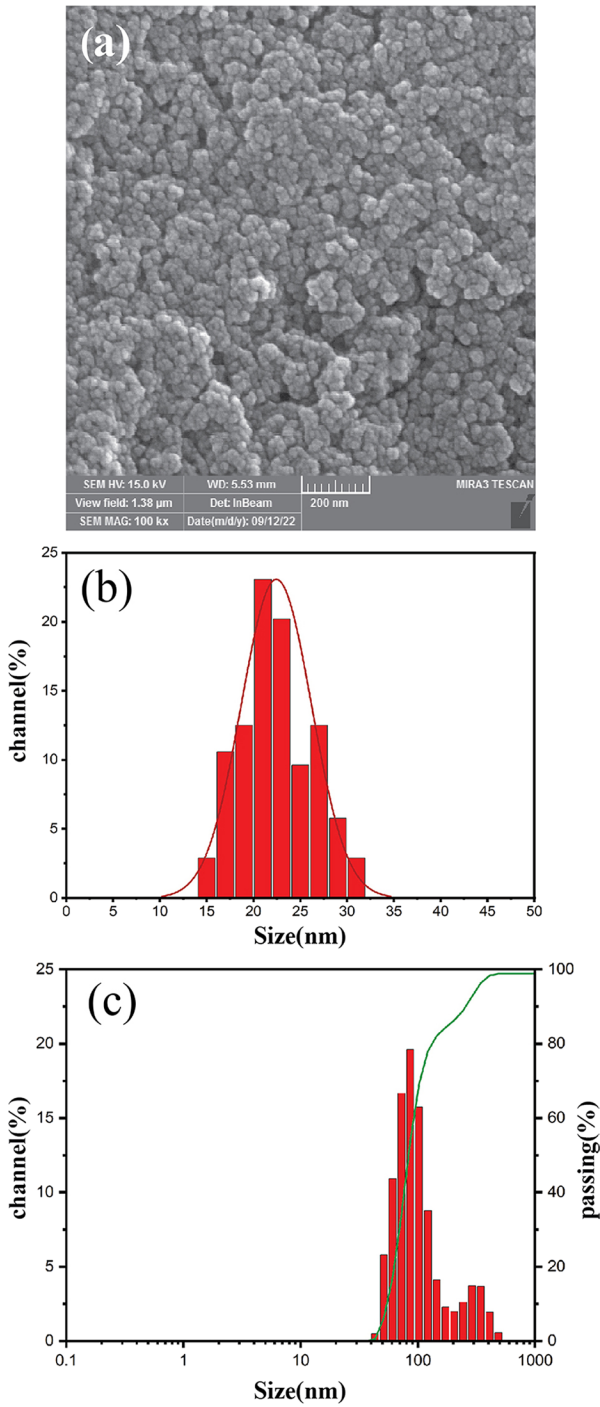## Green synthesis of INPs

Optimization of INPs synthesis

A total of 29 experiments were conducted using the Design Expert software, as outlined in Table S1 in the supplementary material. These experiments closely aligned with the quadratic model, evidenced by a high R^2 value of 0.9860, indicating an excellent fit of the data. The results of the ANOVA test are shown in Table S2 and underscored the significance of variables such as extract pH, volume ratio, and time in the synthesis of INPs, as demonstrated by their low p values (less than 0.0001) and high f values. However, the impact of temperature on INP synthesis was comparatively minimal. Analysis revealed that an increase in extract pH, time, and volume ratio leads to a rise in INP production. The developed model predicts that the optimal conditions for maximum INP yield—0.15 g per reaction—are an extract pH of 9.8, a reaction time of 94 min, a volume ratio of 6, and a temperature of 32 °C. This prediction was substantiated by a validation experiment conducted under these optimal conditions, which confirmed the anticipated INP yield. Further details can be found in the Supplementary material.

Characterization of INPs

The physicochemical properties of the INPs, synthesized under optimal conditions, were thoroughly evaluated. Figure 2a presents both the FESEM images and the corresponding size distribution histogram for these green-synthesized INPs. These FESEM images reveal spherical nanoparticles with diameters ranging from 15 to 31 nm, aligning with findings reported by other researchers [7, 27, 29, 30].

Dynamic light scattering (DLS) analysis was conducted to examine the aggregation tendencies of the INPs in solution [31]. As illustrated in Fig. 2c, the size distribution of the INPs in aqueous solutions ranged between 43 and 489 nm, with an average diameter of approximately 83 nm. This contrasts with the average particle size of 22 nm observed in FESEM images, suggesting a tendency for the INPs to agglomerate. Such agglomeration could be attributed to factors like the solution's form, improper drying, or the Van der Waals forces acting between the particles [30, 31].

Additionally, the zeta potential was measured to assess the stability and surface charge of the INPs in solution. A colloidal dispersion is deemed stable when the particle zeta potential is either above + 30 mV or below -30 mV [32]. The INPs exhibited a zeta potential of -30.4 mV, indicating adequate repulsive forces between

Fig. 2 **a** FESEM image; **b** histogram of particle size distribution; and **c** DLS of the size distribution of green-synthesized INPs

particles and confirming their good colloidal stability in an aqueous solution. The combination of good stability and small diameter underscores the effectiveness of the green method used in nanoparticle synthesis.

The TGA and DTG curves of the synthesized iron nanoparticles are presented in Fig. 3a, revealing a significant weight loss trend. The initial weight loss, occurring at temperatures below 160.9 °C, is associated with the evaporation of residual water in the nanoparticle cavities. The weight loss continuing up to 241.5 °C can be attributed to the decomposition of capping materials [27]. A rapid decomposition of organic material at 282.4 °C leads to the main peak in the DTG curve at this temperature. Notably, no weight loss was observed above 500 °C. TGA analysis indicates that the weight percentage of organic materials serving as stabilizers and coatings is approximately 65.56%. EDS analysis Fig. 3b) confirms the presence of organic compounds in the green-synthesized iron nanoparticles (INPs). Besides iron, the spectrum also displays nitrogen, oxygen, and carbon elements, indicating impurities inherent to the green synthesis process. The respective percentages of Fe, C, O, and N are 7.80, 34.37, 42.59, and 7.25%, aligning with other studies using green synthesis methods.

The FTIR spectrum of the nanoparticles and the green tea extract are depicted in Fig. 4a. The FTIR peaks of the green tea extract in the 3300 cm^{-1} range signify O–H stretching vibrations, while the bond at 1637 cm^{-1} is indicative of polyphenolic compounds arising from the C=C stretching vibration in the aromatic ring. The FTIR spectrum of the nanoparticles also shows stretching vibrations at 3205 cm^{-1} for O–H, 1610 cm^{-1} for C=C, and 1074 cm^{-1} for C–O–C. Peaks at 510 cm^{-1} and 605 cm^{-1} suggest Fe–O stretching vibrations [33, 34], indicating that the polyphenols effectively coat the iron particles, which oxidize upon exposure to air and water.

The XRD pattern of the synthesized iron nanoparticles is illustrated in Fig. 4b. The prominent peak at $2\theta = 23.4°$ signals the presence of organic compounds absorbed from the green tea extract, acting as capping and stabilizing agents for the nanoparticles. The peak at $2\theta = 44.5°$ is indicative of zero-valent iron nanoparticles, while the diffraction peak at $2\theta = 41.6°$ corresponds to the (111) plane, resulting from nanoparticle oxidation. The synthesized nanoparticles comprise two components: a core part and an outer layer of iron oxide [31].
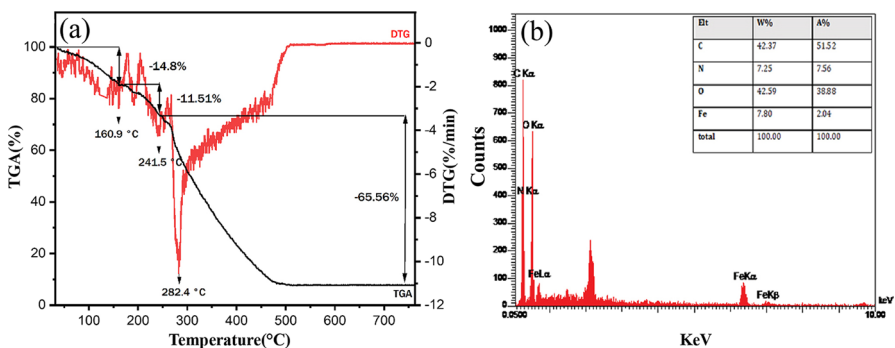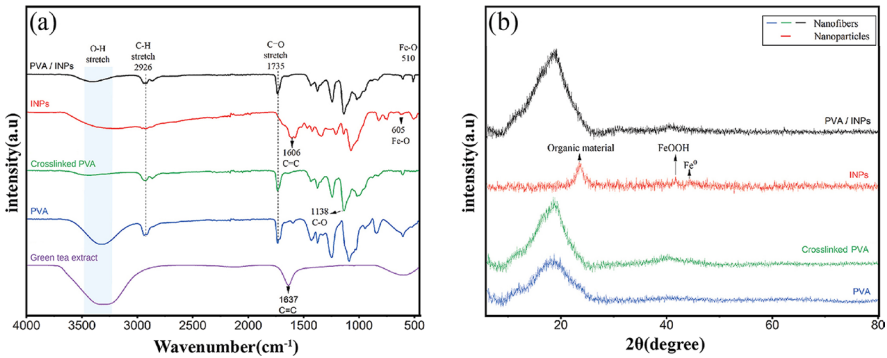

Fig. 3 a TGA and DTG curve and b EDS spectrum of green-synthesized INPs

Fig. 4 **a** FTIR spectra; and **b** X-ray diffraction patterns for green-synthesized INPs, PVA, cross-linked PVA, and PVA/INPs Nanofibers

PVA/INPs nanofiber fabrication

Effect of PVA/INPs nanofiber fabrication method on adsorption efficiency

To determine a more effective preparation method for PVA/INPs (polyvinyl alcohol/iron nanoparticles) nanofibers, we assessed the adsorption capacity and removal efficiency of methylene blue (MB) for each type of nanofiber under identical conditions, with the results detailed in Table 3 These findings indicate that nanofibers produced using the second method exhibited a higher MB adsorption capacity. This enhanced performance is attributed to the increased presence of INPs on the surface of PVA/INP composite nanofibers prepared by method 2, compared to those prepared by method 1. Consequently, the larger surface area of INPs in contact with methylene blue in the composite nanofibers from method 2 accounts for its superior adsorption effectiveness. Subsequent research focused on PVA/INPs nanofibers fabricated using this second method.

Table 3 Adsorption efficiency comparison of fabricated PVA/INPs nanofibers at initial concentration 50 mg/L, nanofiber dose 1.5 g/L, initial pH 6.4, and contact time180 min

Nanofibers	Mb removal (%)	Adsorption capacity (mg/g)
PVA	20.691	3.448
Method 1		
3%INPs	32.903	5.483
4%INPs	35.852	5.975
5%INPs	40.070	6.678
Method 2		
PVA/INPs	67.327	11.221

Characterization of the PVA/INPs nanofibers

The surface morphologies and diameters of uncross-linked PVA, cross-linked PVA, and PVA/INPs (polyvinyl alcohol/iron nanoparticles) nanofibers were examined using FESEM (field-emission scanning electron microscopy), as shown in Fig. 5. Additionally, a histogram depicting their diameter distribution was constructed. The average diameter of uncross-linked PVA nanofibers was measured at 338 ± 62 nm. In comparison, the average diameters for cross-linked PVA and PVA/INPs nanofibers were found to be 380 ± 76 nm and 374 ± 62 nm, respectively. The process of cross-linking with glutaraldehyde vapor caused the nanofiber surfaces to soften, leading to swelling and an increase in thickness [35, 36]. While the synthesis of nanoparticles on the cross-linked PVA nanofibers did not alter their diameter significantly, it did affect their surface roughness due to the formation of nanoparticles on the nanofibers' surface, as evidenced in Fig. 5c.

The FTIR (Fourier transform infrared) spectra of PVA, cross-linked PVA, and PVA/INPs nanofibers, presented in Fig. 4a, were used to assess the cross-linking effectiveness and the accuracy of nanoparticle loading on the nanofibers. Cross-linking predominantly affects the hydroxyl groups in PVA, with cross-linked PVA exhibiting a weaker peak at 3428 cm^{-1} compared to uncross-linked PVA. This change is due to the acetal reaction between glutaraldehyde and PVA, which limits the availability of hydroxyl groups [37]. In contrast, PVA/INPs nanofibers showed a sharper O–H peak compared to cross-linked PVA, attributable to the presence of organic materials from nanoparticles on the nanofiber surfaces. The absorption peak at 510 cm^{-1}, indicative of the stretching vibration
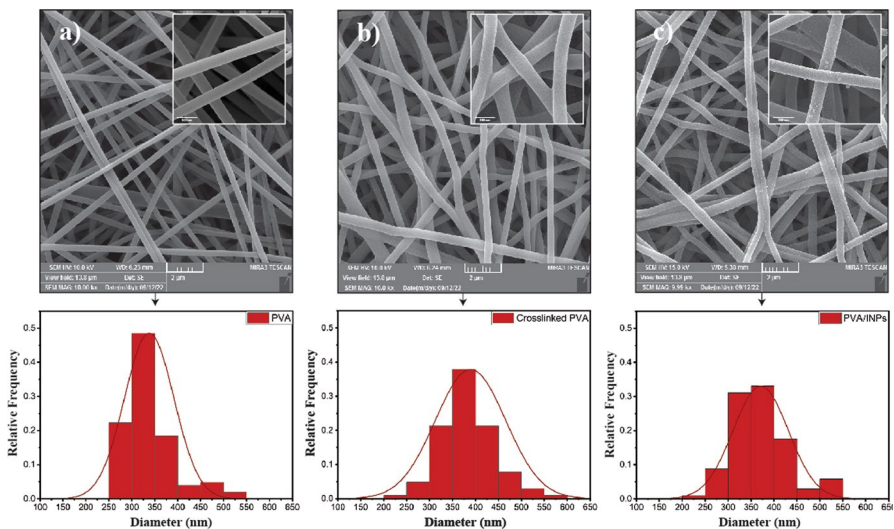
Fig. 5 FESEM image and diameter distribution of nanofibers for **a** PVA; **b** Cross-linked PVA; and **c** PVA/INPs

mode of Fe–O bonds, confirms the presence of nanoparticles synthesized on the nanofibers by the green method [38].

XRD (X-ray diffraction) analysis was used to evaluate the crystallinity of uncross-linked PVA, cross-linked PVA, and PVA/INPs nanofibers. The XRD patterns, shown in Fig. 4b, revealed that all three samples exhibited a characteristic peak around $2\theta = 18.85°$, albeit with varying intensities, which is associated with the PVA matrix. Given that PVA is a semicrystalline polymer, the Scherrer equation can be utilized to estimate the nanofibers' average crystallite size (D).

$$D = \frac{A\lambda}{\Delta\theta cos\theta} \tag{4}$$

Here, the average crystallite size, D, is calculated using Scherrer's formula where A represents the Scherrer constant (value = 1), λ denotes the x-ray wavelength, and $\Delta\theta$ is the full width at half maximum of the angle. Pure polyvinyl alcohol (PVA) nanofibers exhibited a characteristic amorphous phase peak, with a prominent halo at $2\theta = 18.9°$ and an average crystallite size of 12 nm. The crystallinity of these PVA nanofibers was found to increase upon exposure to glutaraldehyde vapors. In cross-linked PVA, two distinct peaks were observed at $2\theta = 19.23°$ and $40.405°$, indicating the formation of a new, more crystalline phase within the PVA structure. The average crystallite sizes for these two phases were measured at 40 nm and 29 nm, respectively. Additionally, PVA nanofibers incorporating iron nanoparticles (PVA/INPs) displayed two peaks at $2\theta = 18.85°$ and $40.835°$, with average crystallite sizes of 28 nm and 37 nm, respectively. This change signifies a decrease in crystallinity within the first phase (PVA matrix) and an increase in the second phase, attributed to the synthesis of iron nanoparticles on the nanofibers, thereby confirming the presence of INPs.

MB adsorption by PVA/INPs nanofibers

MB adsorption mechanism

To clarify the adsorption process, the interactions on PVA/INPs nanofibers were studied using cationic methylene blue dye as the adsorbate. Methylene blue, a cationic dye, contains a quaternary amine group, where the cationic nitrogen interacts with the anionic sites on the synthesized adsorbent through electrostatic interactions. In many cases, the adsorption of dyes onto polyvinyl alcohol-based materials is primarily facilitated by hydrogen bonding involving the nitrogen atoms of the dye molecules (Fig. 6). Additionally, since green tea, which is rich in polyphenols, was utilized in the synthesis of iron nanoparticles, it is likely that the nanoparticles contain aromatic rings. As a result, π-π stacking interactions between the aromatic rings of the polyphenols and methylene blue play a crucial role in the adsorption process. Thus, these interactions are responsible for effective dye removal from an aqueous solution.
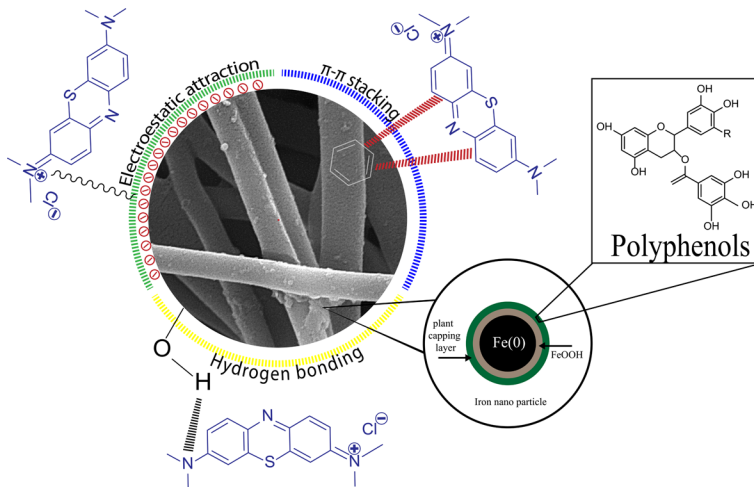
Fig. 6 Proposed mechanism of adsorption of MB dye solution on PVA/INPs nanofibers

Optimization MB adsorption by PVA/INPs nanofibers

The response surface methodology (RSM) is an effective technique for determining the optimum conditions of a process. Among various experimental designs for RSM, the central composite design (CCD) is particularly advantageous for exploring a wide surface area to identify the optimum point. This approach was applied to optimize the adsorption of methylene blue, as detailed in Table 4. Analysis of variance (ANOVA) is employed to evaluate the quality of the selected model. ANOVA identified the quadratic model as the most suitable among various mathematical models, including linear, 2-factor interaction (2Fi), quadratic, and cubic. This selection was based on the model's p value being less than 0.005 and an R-squared value of 0.96, indicating a high level of model fit. The ANOVA results for the experimental data are presented in Table 5, where p values below 0.05 signify significant model terms [39]. ANOVA, four variables—pH, initial methylene blue (MB) concentration, contact time, and the dose of nanofibers—are significant in the model. This model is expressed in coded Eq. 5 to predict the efficiency of MB removal.

$$
\begin{aligned}
MB\,removal\,(\%) \;=\; &74.20 \,+\, 14.33A \,+\, 2.86B \,-\, 5.56C \\
&+\, 13.54D \,-\, 0.4387AB \,+\, 4.39AC \\
&-\, 2.72AD \,-\, 1.46BC \,-\, 4.54BD \\
&-\, 5.48CD \,-\, 6.30A^2 \,-\, 2.09B^2 \\
&+\, 1.19C^2 \,-\, 2.37D^2
\end{aligned}
\tag{5}
$$

where the coded variables A, B, C, and D represent pH, contact time (minutes), initial concentration of methylene blue (MB) (mg/L), and nanofiber dose (g/L),

Table 4 CCD experimental design and response to the dependent variable MB removal percentage

Run	A: pH	B: contact time(min)	C: initial concentration (mg/L) of MB	D: dosage nanofiber (g/L)	Remove percent
1	9	130	40	0.6	80.465 ± 1.06
2	3	90	30	1.1	11.985 ± 1.01
3	5	130	20	1.6	87.201 ± 3.23
4	9	130	20	0.6	70.096 ± 5.72
5	9	50	40	0.6	62.414 ± 1.65
6	7	170	30	1.1	69.121 ± 3.70
7	9	50	20	1.6	91.880 ± 0.62
8	7	90	10	1.1	89.087 ± 0.03
9	7	10	30	1.1	59.527 ± 1.39
10	7	90	30	2.1	94.799 ± 2.02
11	9	50	20	0.6	60.063 ± 1.89
12	7	90	30	1.1	70.639 ± 2.08
13	7	90	30	1.1	73.768 ± 4.55
14	5	50	40	0.6	27.345 ± 3.43
15	7	90	30	1.1	79.294 ± 2.33
16	11	90	30	1.1	82.979 ± 0.69
17	9	50	40	1.6	83.597 ± 2.10
18	7	90	30	1.1	73.647 ± 5.01
19	5	50	20	1.6	81.846 ± 1.79
20	7	90	50	1.1	65.845 ± 4.99
21	5	130	40	0.6	41.613 ± 4.72
22	5	50	40	1.6	59.952 ± 1.68
23	5	130	20	0.6	49.972 ± 0.98
24	7	90	30	1.1	70.169 ± 2.79
25	5	130	40	1.6	42.850 ± 3.01
26	9	130	20	1.6	94.187 ± 3.21
27	7	90	30	1.1	76.710 ± 4.92
28	9	130	40	1.6	81.418 ± 2.58
29	7	90	30	0.01	28.382 ± 1.95
30	5	50	20	0.6	31.302 ± 1.82

respectively. Utilizing this coding, the model was employed to ascertain the optimal conditions for maximum decolorization using PVA/INPs (polyvinyl alcohol/iron nanoparticles) nanofibers. The model identified that at a pH of 8.6, contact time of 100 min, an initial MB concentration of 30 mg/L, and a nanofiber dose of 1.6 g/L, the color removal percentage reached 89%. Validation experiments conducted under these optimal conditions achieved a maximum dye removal efficiency of 85%, confirming the effectiveness of these identified conditions for achieving maximum decolorization.

Table 5 The ANOVA results for the response surface quadratic model for MB dye removal

Source	Sum of squares	df	Mean square	F value	P value	
Model	13146.94	14	939.07	31.94	<0.0001	Significant
A (pH)	4931.42	1	4931.42	167.74	<0.0001	
B (contact time)	196.03	1	196.03	6.67	0.0208	
C (initial concentration of MB)	741.24	1	741.24	25.21	0.0002	
D (dosage of nanofibers)	4511.42	1	4511.42	153.46	<0.0001	
AB	3.08	1	3.08	0.1047	0.7507	
AC	308.26	1	308.26	10.49	0.0055	
AD	118.67	1	118.67	4.04	0.0629	
BC	34.00	1	34.00	1.16	0.2992	
BD	329.80	1	329.80	11.22	0.0044	
CD	480.73	1	480.73	16.35	0.0011	
A^2	1084.62	1	1084.62	36.89	<0.0001	
B^2	119.41	1	119.41	4.06	0.0622	
C^2	38.98	1	38.98	1.33	0.2675	
D^2	179.34	1	179.34	6.10	0.0260	
Residual	440.98	15	29.40			
Lack of fit	379.46	10	37.95	3.08	0.1128	Not significant
Pure error	61.51	5	12.30			
Cor total	13587.92	29				

$R^2 = 0.9675$, Adjusted $R^2 = 0.9373$, Predicted $R^2 = 0.8296$

This study's findings contribute to a broader range of research exploring different levels of adsorption capacity with various nanofiber composites. For instance, Jiang et al. reported a maximum adsorption capacity of 9.25 mg/g using a sodium alginate/PVA composite nanofiber for MB adsorption [40]. Similarly, He, Yao, et al. documented an adsorption capacity of 60.85 mg/g for a PVA/graphene oxide (GO) composite nanofiber, measured at an initial MB concentration of 50 mg/L and a contact time of 2 h [40]. In comparison, the experiments in this study demonstrated an adsorption capacity of 15.93 mg/g under optimal conditions, which was within the range of these previous findings.

Interaction between influencing factors on adsorption

The interaction between two variables in the removal of MB (methylene blue) was investigated using three-dimensional response surface diagrams, as depicted in Fig. 7. These variables were examined in pairs, with all other variables held constant. The interaction between pH and the initial concentration of MB on dye removal is demonstrated in Fig. 7a. MB is cationic dye characterized by positively charged ions in aqueous solutions. An increase in pH leads to a higher removal percentage of MB. This is because as pH rises, negatively charged deprotonated sites increase, enhancing the electrostatic attraction between the adsorbent and MB. Conversely, a decrease in pH results in more protonated adsorption sites,
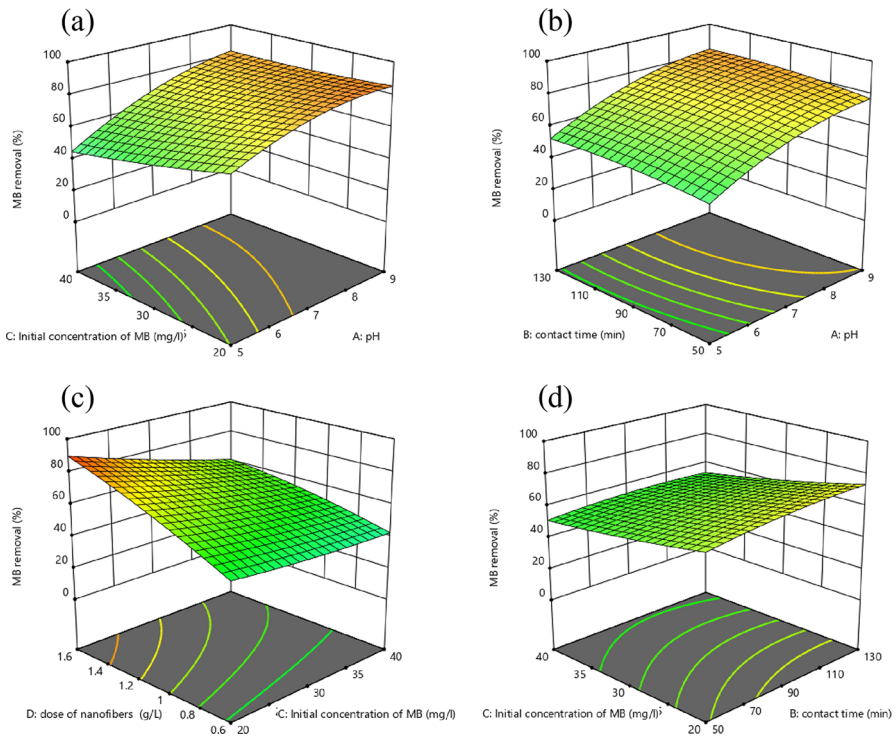
Fig. 7 Response surface plot and interaction between two variables on MB dye removal: **a** interaction between initial concentration of MB and pH; **b** interaction between contact time and pH; **c** interaction between dose of nanofibers and initial concentration

increasing the electrostatic repulsion between the dye and the adsorbent, thereby reducing the removal efficiency of MB [41, 42].

As the initial concentration of MB increases, the removal of MB decreases. The overlap of the active surfaces at high dye concentrations and the reduction of the active surface of PVA/INPs nanofibers cause this phenomenon [43]. Therefore, when the concentration of MB is low and the pH is high, the percentage of MB removal is high.

Figure 7b illustrates the interaction between contact time and pH. According to the ANOVA results, this interaction does not significantly influence the removal of MB, as the p value is above 0.05. The removal efficiency of MB improves with increase in contact time, providing more time for the adsorption of reactive dye molecules [44]. Extended contact time at a high pH also improves dye adsorption by PVA/INPs nanofibers.

Figure 7c displays response surface plots that show the dye removal dependency on the dose of nanofiber and the dye concentration in the solution. Increasing the amount of nanofibers makes more adsorbing and active surfaces available for MB adsorption, thus enhancing the dye removal percentage.

Finally, the effect of contact time and the initial concentration of MB on dye removal is presented in Fig. 7d. This figure indicates that more dye is removed as the contact time increases and the initial dye concentration decreases.

Effect of contact time

To determine the equilibrium time in the adsorption of methylene blue (MB) and to examine more accurately the effect of time on the reaction, experiments were repeated with the concentration of MB in the samples being measured at fifteen-minute intervals. Figure 8 reveals that the adsorption of MB on PVA/INPs nanofibers reaches equilibrium in 90 min. Initially, the removal efficiency escalates rapidly due to the abundance of vacant adsorption sites. Subsequently, the rate of increase in removal efficiency slows down as the number of available adsorption sites decreases [45].

Adsorption kinetic

Various kinetic models were applied to the experimental data concerning the adsorption of MB onto PVA/INPs nanofibers, including pseudo-first-order, pseudo-second-order, Elovich, and intra-particle diffusion models. The linear forms of these kinetic equations are presented in Table 6 [31, 41, 46, 47]. A summary of the results derived from these models is provided in Table 7. The findings indicate that the adsorption of MB on PVA/INPs nanofibers adheres to the pseudo-second-order kinetic model, evidenced by an R^2 value of 0.9961, which surpasses those of the other models. The Elovich model, which describes the interaction between a solid and liquid interface, suggests that an α value greater than β signifies a lower desorption and higher adsorption rates. Therefore, the experimental results demonstrate a strong affinity of MB for adsorption onto PVA/INPs nanofibers [31, 48].

The intra-particle diffusion kinetics, or Weber-Morris model, was employed to identify the reaction pathways, adsorption mechanisms, and predict the
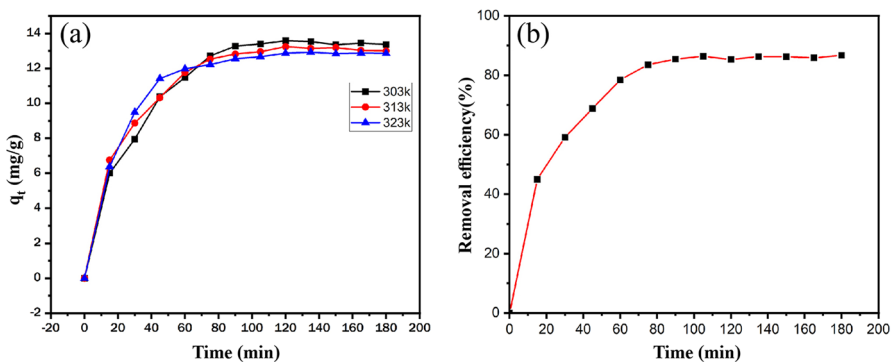
Fig. 8 Plots **a** q_t versus contact time at temperatures 303, 313, and 323K; and **b** MB removal percentage versus contact time at temperature 303 K onto PVA/INPs nanofibers

Table 6 Kinetic models and adsorption isotherms used in this study

	Model	Linear form
Kinetic models	Pseudo-first-order	$\ln(q_e - q_t) = \ln q_e - k_1 t$
	Pseudo-second-order	$\frac{t}{q_t} = \frac{1}{k_2 q_e^2} + \frac{1}{q_e} t$
	Elovich	$q_t = \frac{1}{\beta} \ln A\beta + \frac{1}{B} \ln t$
	Intra-particle-diffusion	$q_t = K_{Id} t^{\frac{1}{2}} + c$
Isotherm models	Langmuir	$\frac{C_e}{q_e} = \frac{1}{q_m k_l} + \frac{C_e}{q_m}$
	Freundlich	$\log q_e = \log k_f + \frac{1}{n} \log C_e$
	Temkin	$q_e = B \ln A + B \ln C_e$
	Harkins–jura	$\frac{1}{q_e^2} = \frac{B}{A} - \frac{1}{A} \log C_e$
	Redlich–peterson	$\ln(K\frac{C_e}{q_e} - 1) = \alpha \ln C_e + \ln b_{RP}$

Table 7 Kinetic parameters for adsorption of the MB dye onto PVA/INPs nanofibers

Exp	Pseudo-first-order			Pseudo-second-order		
$q_{e,exp}(mg/g)$	$q_{e,cal}(mg/g)$	$K_1(min^{-1})$	R^2	$q_{e,cal}(mg/g)$	$K_2(min^{-1})$	R^2
13.247	9.679	0.0328	0.794	14.492	0.0045	0.9961

Elovich			Intra-particle-diffusion		
$\alpha(mg \cdot g/min)$	$\beta(g/mg)$	R^2	$K_{Id}(g/mg.min^{\frac{1}{2}})$	$C(mg/g)$	R^2
2.4770	0.3570	0.9309	0.8246	4.5075	0.8971

rate-controlling step in the process [49].The plot of $t^{0.5}$ versus q did not yield a single linear slope but instead revealed two distinct linear zones. This observation suggests that intra-particle diffusion of the MB dye solution onto PVA/INPs nanofibers is not the sole rate-controlling step, with other mechanisms also playing a role. The presence of two linear regions in the intra-particle diffusion plot indicates that the sorption process involves both surface sorption and intra-particle diffusion. The initial portion of the plot is indicative of the boundary layer effect, while the second linear portion corresponds to intra-particle or pore diffusion [50].

Adsorption isotherm

The adsorption capacity of PVA/INPs nanofibers was assessed using five different adsorption models: Langmuir, Freundlich, Temkin, Harkins–Jura, and Redlich–Peterson, as detailed in Table 8. The linearized equations of these models are presented in Table 6 [41, 51]. The experimental data showed a strong correlation with the Langmuir model, indicated by the highest correlation coefficient

Table 8 Isotherm parameters for adsorption of the MB dye onto PVA/INPs nanofibers

Isotherm model	Parameters	Value
Langmuir	q_m(mg/g)	24.509
	K_L(L/mg)	0.426
	R^2	0.988
Freundlich	K_F(L/mg)	7.212
	n	2.059
	R^2	0.961
Temkin	$A(L/g)$	4.538
	B	5.221
	R^2	0.984
Harkins–Jura	A	32.679
	B	0.862
	R^2	0.759
Redlich–Peterson	K	14.92
	b_{RP}	0.952
	α	0.825
	R^2	0.971

(R^2) among the models. This result suggests that MB molecules are adsorbed onto the surface of the nanofibers through monolayer adsorption. The maximum adsorption capacity (max) determined by this model was 24.509 mg/g.

Temkin model considers that the heat of adsorption of the molecules in the layer reduces linearly with the coverage because of the interactions between adsorbent and adsorbate. From the data presented in Table 8, the Temkin isotherm model yielded an R^2 value of 0.984, indicating a strong correlation with the experimental data. The Temkin isotherm equilibrium binding constant (A) was determined to be 4.538. Additionally, the Temkin constant (B), which is associated with the heat of methylene blue (MB) adsorption on PVA/INPs nanofibers, was calculated to be 5.221 J/mol. The fact that the B value obtained from the Temkin model is greater than 1 suggests that electrostatic interactions are significant in the adsorption process. Furthermore, it implies that pore heterogeneity on the surface of the PVA/INPs nanofibers plays a crucial role in the adsorption of MB [52].

The Redlich–Peterson (R–P) isotherm model describes a homogeneous monolayer adsorption process, characterized by constant enthalpies and adsorption energies. This model effectively addresses the limitations associated with the two-parameter Langmuir and Freundlich isotherm equations in certain adsorption systems. The three-parameter R–P isotherm equation simplifies to the Langmuir isotherm when the isotherm exponent (α) approaches 1, whereas when the b value approaches 0, it becomes complementary to the Freundlich isotherm [53]. In this study, fitting the experimental data to the R–P isotherm model resulted in a high correlation coefficient (R^2) of 0.971, suggesting a strong fit between the model and the observed data. The isotherm exponent (α) was found to be 0.865, which indicates that the adsorption of methylene blue (MB) onto PVA/INPs nanofibers aligns more closely with the

Langmuir model than with the Freundlich model. This suggests that the adsorption process is likely dominated by monolayer coverage on a relatively uniform surface, where all adsorption sites are equivalent in terms of energy [54].

Thermodynamic studies

To ascertain the thermodynamic parameters of the adsorption process of MB by PVA/INPs nanofibers, experiments were conducted at varying temperatures, 30, 40, and 50 °C, under optimal conditions. The results are depicted in Fig. 8a. For this purpose, the plot of $\ln(q_e/c_e)$ versus T^{-1} was drawn based on Eq. 6 using the experimental data. The values of ΔH (enthalpy change) and ΔS (entropy change) for the adsorption process were calculated from the slope and intercept of this plot.

$$ln\frac{q_e}{c_e} = -\frac{\Delta H}{RT} + \frac{\Delta S}{R} \tag{6}$$

The value of ΔG for different temperatures was obtained from Eq. 7, and the thermodynamic parameters are reported in Table 9.

$$\Delta G = \Delta H - T\Delta S \tag{7}$$

where R represents the universal gas constant (8.314 J/mol K) and T denotes the absolute temperature (K). ΔG is the Gibbs free energy of sorption (kJ/mol), while ΔH (kJ/mol) and ΔS (J/mol·K), respectively, signify the enthalpy and entropy of sorption. The results revealed that ΔG was negative at all three temperatures, suggesting that methylene blue (MB) adsorption onto PVA/INPs nanofibers occurs spontaneously. The nature of the MB adsorption process is exothermic, as indicated by the negative enthalpy value. A negative ΔS value implies a decrease in randomness due to the interaction between the adsorbate and adsorbent [45].

Reusability

The reusability and recovery of the synthesized adsorbent are critical factors in assessing the potential of PVA/INPs for industrial applications. The dye-loaded PVA/INPs adsorbents were regenerated by rinsing with an ethanol solution. The recyclability of the used adsorbents, as depicted in Fig. 9, indicates that the removal efficiency of methylene blue (MB) by PVA/INPs adsorbent decreases slightly with each adsorption cycle. This slight decline suggests effective regeneration of the spent adsorbents. Notably, even after five adsorption cycles, the regenerated PVA/

Table 9 Thermodynamic parameters for MB adsorption on PVA/INPs at different temperatures

Temperature (K)	ΔG (kJ /mol)	ΔH (kJ/mol)	ΔS(J /mol)
303	− 33.51		
313	− 28.11	− 16.68	− 43.99
323	− 24.71		
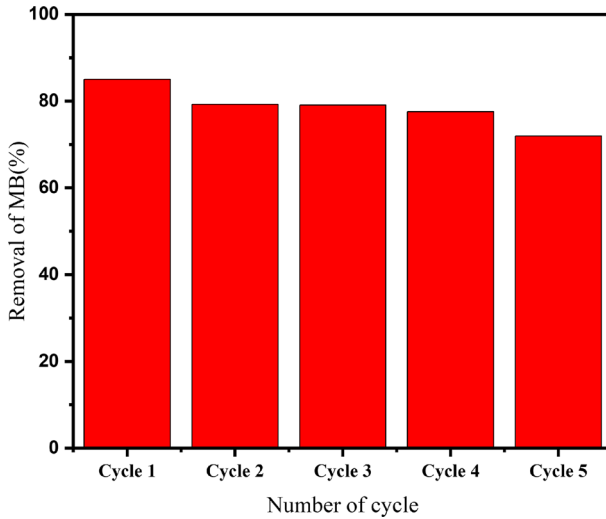
Fig. 9 Regeneration and reusability for PVA/INPs nanofibers after five cycles using ethanol solution

INPs adsorbent maintained a relatively high removal efficiency of 72% for cationic MB dye, demonstrating the practicality and durability of PVA/INPs adsorbents for repeated use in industrial settings.

Evaluation of performance

In Table 10, the adsorption capacities (q_e) of various PVA-based polymer composite adsorbents for methylene blue (MB) removal, as reported in the literature, are summarized. It is noteworthy that the nanofiber adsorbent developed

Table 10 Comparison of the equilibrium adsorption capacity for methylene blue dye on PVA-based adsorbents reported in the literature

Adsorbent	Maximum adsorption capacity (mg/g)	References
Sodium alginate/PVA	9.25	[47]
PVA/PAA/GO-COOH@PDA	27	[55]
Ce-UiO-66 into the PVA/CTS matrix	1111	[56]
PEI/PVA	209.63	[57]
PVA/carboxymethyl cellulose/ ZSM-5 zeolite	7.8	[58]
(PVA-SS-CD)	261	[59]
MI-SS/PVA	223	[60]
CS/PVP/PVA	13.27	[61]
PVA/CMC/PEO	11.45	[62]
PVA/INPs	24.50	This work

in this study demonstrates a respectable adsorption capacity (q_e), particularly given the simplicity of its fabrication, in comparison with other recently reported adsorbents. However, the q_e values calculated in this work are lower than those observed for PVA/PEI nanofibers, polyvinyl alcohol nanofibers containing sericin/β-cyclodextrin, imprinted sericin/polyvinyl alcohol adsorbents, and PVA/chitosan nanofibers embedded with Ce-UiO-66 nanoparticles. Despite this, an analysis of the cost (Table S3) and ease of fabrication of this type of adsorbent indicate that its economic efficiency could potentially offset the lower adsorption capacity when compared to the aforementioned alternatives.

Conclusions

This study presents a novel approach for the preparation of polyvinyl alcohol (PVA) nanofibers embedded with iron nanoparticles (INPs) through an environmentally friendly green synthesis method. Iron nanoparticles were synthesized using green tea leaf extract, and their production was optimized through response surface methodology (RSM) based on central composite design (CCD). The model predicted a maximum production of 0.15 g of iron nanoparticles per reaction (4.285 mg/ml of the reaction mixture), achieved under optimal conditions: volume ratio (6) (5 ml of ferrous sulfate heptahydrate 0.1 M and 30 ml green tea extract), pH (9.8), reaction time (98 min), and temperature (32 °C). The synthesized nanoparticles had an average diameter of 22 nm. The PVA/INPs nanofibers, with an average diameter of 389 nm, achieved an MB removal rate of 85% from aqueous solutions under optimal conditions, including a pH of 8.6, an initial MB concentration of 30 mg/L, a nanofiber dose of 1.6 g/L, and a contact time of 100 min. The kinetic model analysis revealed an equilibrium adsorption capacity of 14.492 mg/g, with a maximum adsorption capacity of 24.509 mg/g. The negative values of Gibbs free energy and adsorption enthalpy indicate that the adsorption process is both spontaneous and exothermic. These results demonstrate that the PVA/INPs nanofiber membranes developed through this innovative green synthesis method are highly effective for the removal of methylene blue from wastewater. This advancement offers a promising solution for addressing dye pollution in the textile and dye industries.

Declarations

Conflict of interest The authors have no relevant financial or nonfinancial interests to disclose.

References

1. Oladoye PO, Ajiboye TO, Omotola EO, Oyewola OJ (2022) Methylene blue dye: toxicity and potential elimination technology from wastewater. Results Eng 16:100678. https://doi.org/10.1016/j.rineng.2022.100678

2. Nourozi S, Zare-Dorabei R (2017) Highly efficient ultrasonic-assisted removal of methylene blue from aqueous media by magnetic mesoporous silica: experimental design methodology, kinetic and equilibrium studies. Desalin Water Treat 85:184–196. https://doi.org/10.5004/dwt.2017.21207

3. Ramezani F, Zare-Dorabei R (2019) Simultaneous ultrasonic-assisted removal of malachite green and methylene blue from aqueous solution by Zr-SBA-15. Polyhedron 166:153–161. https://doi.org/10.1016/j.poly.2019.03.033

4. Tehrani MS, Zare-Dorabei R (2016) Highly efficient simultaneous ultrasonic-assisted adsorption of methylene blue and rhodamine B onto metal organic framework MIL-68 (Al): central composite design optimization. RSC Adv 6:27416–27425. https://doi.org/10.1039/C5RA28052D

5. Tehrani MS, Zare-Dorabei R (2016) Competitive removal of hazardous dyes from aqueous solution by MIL-68(Al): Derivative spectrophotometric method and response surface methodology approach. Spectrochim Acta A Mol Biomol Spectrosc 160:8–18. https://doi.org/10.1016/j.saa.2016.02.002

6. Elzain AA, El-Aassar M, Hashem F et al (2019) Removal of methylene dye using composites of poly (styrene-co-acrylonitrile) nanofibers impregnated with adsorbent materials. J Mol Liq 291:111335. https://doi.org/10.1016/j.molliq.2019.111335

7. Wang T, Lin J, Chen Z et al (2014) Green synthesized iron nanoparticles by green tea and eucalyptus leaves extracts used for removal of nitrate in aqueous solution. J Clean Prod 83:413–419. https://doi.org/10.1016/j.jclepro.2014.07.006

8. Varghese RJ, Zikalala N, Oluwafemi OS (2020) Green synthesis protocol on metal oxide nanoparticles using plant extracts, in Colloidal metal oxide nanoparticles, Elsevier. 67–82.

9. Iqbal A, Haq Au, Cerrón-Calle GA et al (2021) Green synthesis of flower-shaped copper oxide and nickel oxide nanoparticles via Capparis decidua leaf extract for synergic adsorption-photocatalytic degradation of pesticides. Catalysts 11:806. https://doi.org/10.3390/catal11070806

10. Parshetti GK, Doong RA (2009) Dechlorination of trichloroethylene by Ni/Fe nanoparticles immobilized in PEG/PVDF and PEG/nylon 66 membranes. Water Res 43:3086–3094. https://doi.org/10.1016/j.watres.2009.04.037

11. Islam MS, Hernandez S, Wan H et al (2018) Role of membrane pore polymerization conditions for pH responsive behavior, catalytic metal nanoparticle synthesis, and PCB degradation. J Memb Sci 555:348–361. https://doi.org/10.1016/j.memsci.2018.03.060

12. Patel S, Hota G (2016) Iron oxide nanoparticle-immobilized PAN nanofibers: synthesis and adsorption studies. RSC Adv 6:15402–15414. https://doi.org/10.1039/C5RA20345G

13. El-Aswar EI, Ramadan H, Elkik H, Taha AG (2022) A comprehensive review on preparation, functionalization and recent applications of nanofiber membranes in wastewater treatment. J Environ Manage 301:113908. https://doi.org/10.1016/j.jenvman.2021.113908

14. Liu Q, Zhong LB, Zhao QB et al (2015) Synthesis of Fe3O4/polyacrylonitrile composite electrospun nanofiber mat for effective adsorption of tetracycline. ACS Appl Mater Interfaces 7:14573–14583. https://doi.org/10.1021/acsami.5b04598

15. Rezaei V, Mirzaei E, Taghizadeh S-M et al (2021) Nano iron oxide-PCL composite as an improved soft tissue scaffold. Processes 9:1559. https://doi.org/10.3390/pr9091559

16. Ren J, Woo YC, Yao M et al (2017) Enhancement of nanoscale zero-valent iron immobilization onto electrospun polymeric nanofiber mats for groundwater remediation. Process Saf Environ Prot 112:200–208. https://doi.org/10.1016/j.psep.2017.04.027

17. Kharaghani D, Lee H, Ishikawa T et al (2019) Comparison of fabrication methods for the effective loading of Ag onto PVA nanofibers. Text Res J 89:625–634. https://doi.org/10.1177/0040517517753635

18. Kharaghani D, Khan MQ, Tamada Y et al (2018) Fabrication of electrospun antibacterial PVA/Cs nanofibers loaded with CuNPs and AgNPs by an in-situ method. Polym Testing 72:315–321. https://doi.org/10.1016/j.polymertesting.2018.10.029

19. Bayat A, Tati A, Ahmadipouya S et al (2021) Electrospun chitosan/polyvinyl alcohol nanocomposite holding polyaniline/silica hybrid nanostructures: an efficient adsorbent of dye from aqueous solutions. J Mol Liq 331:115734. https://doi.org/10.1016/j.molliq.2021.115734

20. Osei L, Fosu S, Ndur S (2024) Sorption of mercury from water by green synthesised silver nanoparticles supported on natural rubber latex/polyvinyl alcohol nanofibre. Int J Environ Sci Technol 21:4223–4238. https://doi.org/10.1007/s13762-023-05282-0

21. Ghalei S, Asadi H, Ghalei B (2018) Zein nanoparticle-embedded electrospun PVA nanofibers as wound dressing for topical delivery of anti-inflammatory diclofenac. J Appl Polym Sci 135:46643. https://doi.org/10.1002/app.46643

22. Saallah S, Naim MN, Lenggoro IW et al (2016) Immobilisation of cyclodextrin glucanotransferase into polyvinyl alcohol (PVA) nanofibres via electrospinning. Biotechnol Rep 10:44–48. https://doi.org/10.1016/j.btre.2016.03.003

23. Radoor S, Karayil J, Parameswaranpillai J, Siengchin S (2020) Adsorption of methylene blue dye from aqueous solution by a novel PVA/CMC/halloysite nanoclay bio composite: Characterization, kinetics, isotherm and antibacterial properties. J Environ Health Sci Eng 18:1311–1327. https://doi.org/10.1007/s40201-020-00549-x

24. Ibupoto AS, Qureshi UA, Ahmed F et al (2018) Reusable carbon nanofibers for efficient removal of methylene blue from aqueous solution. Chem Eng Res Des 136:744–752. https://doi.org/10.1016/j.cherd.2018.06.035

25. Igwegbe CA, Mohmmadi L, Ahmadi S et al (2019) Modeling of adsorption of methylene blue dye on Ho-CaWO(4) nanoparticles using response surface methodology (RSM) and artificial neural network (ANN) techniques. MethodsX 6:1779–1797. https://doi.org/10.1016/j.mex.2019.07.016

26. Prema P, Veeramanikandan V, Rameshkumar K et al (2022) Statistical optimization of silver nanoparticle synthesis by green tea extract and its efficacy on colorimetric detection of mercury from industrial waste water. Environ Res 204:111915. https://doi.org/10.1016/j.envres.2021.111915

27. Kheshtzar R, Berenjian A, Taghizadeh S-M et al (2019) Optimization of reaction parameters for the green synthesis of zero valent iron nanoparticles using pine tree needles. Green Process Synth 8:846–855. https://doi.org/10.1515/gps-2019-0055

28. Haider S, Uddin Khan S, Najeeb J et al (2022) Synthesis of cadmium oxide nanostructures by using Dalbergia sissoo for response surface methodology based photocatalytic degradation of methylene blue. J Clean Prod 365:132822. https://doi.org/10.1016/j.jclepro.2022.132822

29. Jain R, Mendiratta S, Kumar L, Srivastava A (2021) Green synthesis of iron nanoparticles using Artocarpus heterophyllus peel extract and their application as a heterogeneous Fenton-like catalyst for the degradation of Fuchsin Basic dye. Curr Res Green Sustain Chem 4:100086. https://doi.org/10.1016/j.crgsc.2021.100086

30. Wang T, Jin X, Chen Z et al (2014) Green synthesis of Fe nanoparticles using eucalyptus leaf extracts for treatment of eutrophic wastewater. Sci Total Environ 466–467:210–213. https://doi.org/10.1016/j.scitotenv.2013.07.022

31. Abdelfatah AM, Fawzy M, Eltaweil AS, El-Khouly ME (2021) Green synthesis of nano-zero-valent iron using ricinus communis seeds extract: Characterization and application in the treatment of methylene blue-polluted water. ACS Omega, voi 6, pp 25397–25411 https://doi.org/10.1021/acsomega.1c03355.

32. Nayak D, Ashe S, Rauta PR et al (2016) Bark extract mediated green synthesis of silver nanoparticles: evaluation of antimicrobial activity and antiproliferative response against osteosarcoma. Mater Sci Eng C Mater Biol Appl 58:44–52. https://doi.org/10.1016/j.msec.2015.08.022

33. Hamzezadeh A, Fazlzadeh M, Rahmani K, Poureshgh Y (2021) A novel green synthesis of zero valent iron nanoparticles (nZVI) using walnut green skin: characterisation, catalytic degradation and toxicity studies. International Journal of Environmental Analytical Chemistry, https://doi.org/10.21203/rs.3.rs-372024/v1.

34. Zha S, Cheng Y, Gao Y et al (2014) Nanoscale zero-valent iron as a catalyst for heterogeneous Fenton oxidation of amoxicillin. Chem Eng J 255:141–148. https://doi.org/10.1016/j.cej.2014.06.057

35. Baykara D, Pilavci E, Cesur S et al (2023) Controlled release of gentamicin from electrospun Poly (Vinyl Alcohol)/gelatin nanofibers: The effect of crosslinking time using glutaraldehyde vapor. ChemistrySelect 8:e202203681. https://doi.org/10.1002/slct.202203681

36. Destaye AG, Lin CK, Lee CK (2013) Glutaraldehyde vapor cross-linked nanofibrous PVA mat with in situ formed silver nanoparticles. ACS Appl Mater Interfaces 5:4745–4752. https://doi.org/10.1021/am401730x

37. Ullah S, Hashmi M, Hussain N et al (2020) Stabilized nanofibers of polyvinyl alcohol (PVA) crosslinked by unique method for efficient removal of heavy metal ions. J Water Process Eng 33:101111. https://doi.org/10.1016/j.jwpe.2019.101111

38. Iram M, Guo C, Guan Y et al (2010) Adsorption and magnetic removal of neutral red dye from aqueous solution using Fe3O4 hollow nanospheres. J Hazard Mater 181:1039–1050. https://doi.org/10.1016/j.jhazmat.2010.05.119

39. Igwegbe CA, Mohmmadi L, Ahmadi S et al (2019) Modeling of adsorption of methylene blue dye on Ho-CaWO4 nanoparticles using response surface methodology (RSM) and artificial neural network (ANN) techniques. MethodsX 6:1779–1797. https://doi.org/10.1016/j.mex.2019.07.016

40. He Y, Tian H, Xiang A et al (2022) Fabrication of PVA/GO nanofiber films by electrospinning: application for the adsorption of cu2+ and organic dyes. J Polym Environ 30:2964–2975. https://doi.org/10.1007/s10924-021-02366-1

41. Moradi E, Ebrahimzadeh H, Mehrani Z, Asgharinezhad AA (2019) The efficient removal of methylene blue from water samples using three-dimensional poly (vinyl alcohol)/starch nanofiber membrane as a green nanosorbent. Environ Sci Pollut Res 26:35071–35081. https://doi.org/10.1007/s11356-019-06400-7

42. Dutta S, Saha R, Kalita H, Bezbaruah AN (2016) Rapid reductive degradation of azo and anthraquinone dyes by nanoscale zero-valent iron. Environ Technol Innov 5:176–187. https://doi.org/10.1002/slct.202203681

43. Mahmoodi NM, Oveisi M, Taghizadeh A, Taghizadeh M (2020) Synthesis of pearl necklace-like ZIF-8@chitosan/PVA nanofiber with synergistic effect for recycling aqueous dye removal. Carbohydr Polym 227:115364. https://doi.org/10.1016/j.carbpol.2019.115364

44. Fan J, Guo Y, Wang J, Fan M (2009) Rapid decolorization of azo dye methyl orange in aqueous solution by nanoscale zerovalent iron particles. J Hazard Mater 166:904–910. https://doi.org/10.1016/j.jhazmat.2008.11.091

45. El-Shamy AG (2020) An efficient removal of methylene blue dye by adsorption onto carbon dot@zinc peroxide embedded poly vinyl alcohol (PVA/CZnO2) nano-composite: a novel reusable adsorbent. Polymer 202:122565. https://doi.org/10.1016/j.polymer.2020.122565

46. Goscianska J, Fathy NA, Aboelenin RMM (2017) Adsorption of solophenyl red 3BL polyazo dye onto amine-functionalized mesoporous carbons. J Colloid Interface Sci 505:593–604. https://doi.org/10.1016/j.jcis.2017.06.052

47. Jiang X, Sang C, Wang J, Guo J (2022) Preparation of sodium alginate/polyvinyl alcohol composite nanofiber membranes for adsorption of dyes. Text Res J 92:3154–3163

48. Ahamad K, Singh R, Baruah I et al (2018) Equilibrium and kinetics modeling of fluoride adsorption onto activated alumina, alum and brick powder. Groundw Sustain Dev 7:452–458. https://doi.org/10.1016/j.gsd.2018.06.005

49. Oyarce E, Cantero-López P, Roa K et al (2023) Removal of highly concentrated methylene blue dye by cellulose nanofiber biocomposites. Int J Biol Macromol 238:124045. https://doi.org/10.1016/j.ijbiomac.2023.124045

50. Mahmoodi NM, Mokhtari-Shourijeh Z (2015) Preparation of PVA-chitosan blend nanofiber and its dye removal ability from colored wastewater. Fibers Polym 16:1861–1869. https://doi.org/10.1007/s12221-015-5371-1

51. Aydin YA (2021) Fabrication of chitosan/polyvinyl alcohol/amine modified carbon nanotube composite films for rapid chromate removal. J Appl Polym Sci 138:50339. https://doi.org/10.1002/app.50339

52. Martins AC, Pezoti O, Cazetta AL et al (2015) Removal of tetracycline by NaOH-activated carbon produced from macadamia nut shells: kinetic and equilibrium studies. Chem Eng J 260:291–299. https://doi.org/10.1016/j.cej.2014.09.017

53. Wu F-C, Liu B-L, Wu K-T, Tseng R-L (2010) A new linear form analysis of Redlich-Peterson isotherm equation for the adsorptions of dyes. Chem Eng J 162:21–27. https://doi.org/10.1016/j.cej.2010.03.006

54. Foo KY, Hameed BH (2010) Insights into the modeling of adsorption isotherm systems. Chem Eng J 156:2–10. https://doi.org/10.1016/j.cej.2009.09.013

55. Ruirui X, Wei W, Tifeng J, et al (2017) Bioinspired Polydopamine Sheathed Nanofibers Containing Carboxylate Graphene Oxide Nanosheet for High-Efficient Dyes Scavenger.

56. Tati A, Ahmadipouya S, Molavi H et al (2023) Efficient removal of organic dyes using electrospun nanofibers with Ce-based UiO-66 MOFs. Ecotoxicol Environ Saf 266:115584. https://doi.org/10.1016/j.ecoenv.2023.115584

57. Fang X, Xiao S, Shen M et al (2011) Fabrication and characterization of water-stable electrospun polyethyleneimine/polyvinyl alcohol nanofibers with super dye sorption capability. New J Chem 35:360–368. https://doi.org/10.1039/C0NJ00764A

58. Sabarish R, Unnikrishnan G (2018) Polyvinyl alcohol/carboxymethyl cellulose/ZSM-5 zeolite bio-composite membranes for dye adsorption applications. Carbohyd Polym 199:129–140. https://doi.org/10.1016/j.carbpol.2018.06.123

59. Zhao R, Wang Y, Li X et al (2015) Water-insoluble sericin/β-cyclodextrin/PVA composite electrospun nanofibers as effective adsorbents towards methylene blue. Colloids Surf, B 136:375–382. https://doi.org/10.1016/j.colsurfb.2015.09.038

60. Zhao R, Li X, Sun B et al (2017) Preparation of molecularly imprinted sericin/poly (vinyl alcohol) electrospun fibers for selective removal of methylene blue. Chem Res Chin Univ 33:986–994. https://doi.org/10.1007/s40242-017-7115-9

61. Wu S, Li K, Shi W, Cai J (2022) Preparation and performance evaluation of chitosan/polyvinylpyrrolidone/polyvinyl alcohol electrospun nanofiber membrane for heavy metal ions and organic pollutants removal. Int J Biol Macromol 210:76–84. https://doi.org/10.1016/j.ijbiomac.2022.05.017

62. Zhang C, Wang R, Zhang L et al (2023) Self-assembled electrospun PVA/CMC/PEO composite fiber film material with enhanced dye adsorption performance for wastewater treatment. Colloids Surf, A 678:132461. https://doi.org/10.1016/j.colsurfa.2023.132461